Juin 1986

LRP 296/86

OBSERVATION OF DENSITY FLUCTUATIONS AT THE RESONANCE LAYERS DURING ALFVEN WAVE HEATING

R.Behn, G.A. Collins, J.B. Lister and H. Weisen

Submitted for publication to Plasma Physics and Controlled Fusion

OBSERVATION OF DENSITY FLUCTUATIONS AT THE RESONANCE LAYERS DURING ALFVEN WAVE HEATING

R. Behn, G.A. Collins, J.B. Lister and H. Weisen

Centre de Recherches en Physique des Plasmas
Association Euratom - Confédération Suisse
Ecole Polytechnique Fédérale de Lausanne
21, Av. des Bains, CH-1007 Lausanne / Switzerland

Abstract

We report on the first observations of driven density fluctuations at the resonant layers during Alfvén Wave heating in a tokamak. Whereas loading and external magnetic probe measurements show excellent agreement with the cold plasma model of the Shear Alfvén Wave if finite ω/ω_{ci} effects and toroidal coupling are taken into account, the new results demonstrate the importance of kinetic effects.

1. INTRODUCTION

The resonant absorption of Shear Alfvén Waves for heating a tokamak plasma is currently under study on the TCA tokamak ($R,a = 0.61, 0.18m$, $B_\phi \leq 1.5$ T, $n_e(0) \leq 1.8 \times 10^{20}$ m^{-3}, $I_p \leq 170$ kA). This method of plasma heating relies on driving a plasma resonance which satifies the condition $\omega = k_\parallel v_A$, expressed in the large aspect ratio approximation as

$$\omega^2_{(r)} = \frac{(n+m/q(r))^2 B_\phi^2}{\mu_o \rho(r) R_o^2} (1 - \omega^2/\omega_{ci}^2) \qquad (1)$$

where n,m are the toroidal and poloidal mode numbers, q(r) is the local value of the safety factor, B_ϕ is the toroidal magnetic field, $\rho(r)$ is the local mass density and R_o is the major radius. In TCA the excited mode numbers are selected by the relative phasings of the eight antenna groups, four equally spaced at the top and four at the bottom of the vacuum vessel. The launching of Shear Alfvén Waves in a tokamak geometry has been extensively studied using a cold plasma model (see APPERT et al. (1986) for a bibliography). The experimental results from TCA on antenna loading and rf wavefield measurements showed the importance of the equilibrium current, the finite frequency terms ($\omega/\omega_{ci} \neq 0$) and the toroidal geometry; these studies are described in detail by COLLINS et al. (1986).

The cold plasma theory describes the damping of the fast magnetosonic wave by the localised absorption of the wave power at the Shear Alfvén Wave resonance layers defined by equation (1). When kinetic effects are included the wave solution is dramatically changed, mainly

by the appearance of a radially propagating wave possessing an electrostatic component ($E_\parallel \neq 0$) with an accompanying local density modulation.

The properties of this Kinetic Alfvén Wave (KAW) were first studied by HASEGAWA and CHEN (1975), who derived a wave equation for the KAW in planar geometry for a shearless magnetised plasma with a non-uniform density profile. Under typical tokamak conditions with $v_e > v_A$ corresponding to $\beta > m_e/m_i$, the direction of propagation was predicted to be in the direction of increasing density. In these conditions the KAW's are expected to be heavily electron Landau damped, with attenuation lengths comparable with the wavelengths. The short damping length together with the non-uniformity of the plasma prevent the definition of a wavenumber in the strict sense as well as the use of a uniform plasma dispersion relation near the resonant surfaces, where the wave amplitude is largest. We may however broadly define a wavelength as the distance required by the wave to complete a full cycle. From the WKB approximation (HASEGAWA and CHEN, 1976) we estimate this wavelength Λ in the vicinity of the resonant layer to be

$$\Lambda \sim (3\pi\rho_s)^{2/3} \kappa^{-1/3} \qquad (2)$$

where $\rho_s = \rho_i[3/4 + T_e/T_i]$

$\kappa = \nabla n_e/n_e$

and ρ_i is the ion Larmor radius.

Numerical calculations in cylindrical geometry by ROSS et al. (1982) and DONNELLY et al. (1985b) have shown that the KAW propagates

radially inward for $\beta > m_e/m_i$ and that its amplitude peaks near the calculated positions of the Shear Alfvén Wave resonances. The presence of the electrostatic component is not easily detectable outside the plasma column by probes, except in some extreme cases as shown in the two studies referenced above. Calculations by DONNELLY et al. (1986a) suggest that these surface modes would not be detectable in a plasma with a smooth decay of the density between the limiter radius and the conducting wall. Consequently, a measurement sensitive to the density fluctuations due to the KAW inside the plasma column is called for.

Alfvén wave heating experiments on TCA reported by JOYE et al. (1986) show that the heat deposition profile is more peaked than would be expected if the power was deposited only at the resonance layers. These authors raised the question wether the KAW could be responsible for transporting the energy towards the centre from the resonance layers.

2. EXPERIMENTAL LAYOUT

The TCA tokamak has been equipped with a novel laser diagnostic based on the phase contrast method (WEISEN, 1985a, 1985b, 1986). This instrument uses an 8 Watt CO_2 laser beam (λ = 10.6 μ) expanded to fill 23 × 4 cm wide NaCl windows giving access to the outer two thirds of a poloidal section of the plasma. The transmitted light is optically processed to produce an image of the plasma, in which the small ($\lesssim 10^{-3}$) phase shifts caused by refractive perturbations are revealed as intensity variations, recorded by HgCdTe detectors (Fig. 1). Even

though it needs no external reference beam, this method provides a response equivalent to that of an interferometer, for fluctuations with wavelengths below an adjustable cutoff Λ_c ($\Lambda_c \leq$ 20cm). This is adequate for wavelengths in the centimetric range, as predicted (Eq. 2) for the Kinetic Alfvén Wave in the conditions of TCA, typically $T_e(0) \simeq 800$ eV, $\bar{n}_e = 2\text{-}6 \cdot 10^{19} m^{-3}$, $B_0 = 1.5$ T.

For $r \gg \Lambda$, where $\Lambda = 2\pi/k_r$ is the radial wavelength, a reliable estimate of the local fluctuation amplitude a(r) can be obtained without the need for an Abel inversion. For this purpose we use the approximation

$$\int a(r) \exp(ik_r r - \omega t) dz \simeq \sqrt{\Lambda r}\, a(x) \exp(ik_r r + \pi/4 - \omega t) \quad (3)$$

where the envelope a(r) of the fluctuations, is assumed to be slowly varying with r, as compared with $\exp(ik_r r)$, and $r = (x^2+z^2)^{1/2}$ is approximated by $r \simeq |x + z^2/2x|$.

The fluctuations are detected synchronously with the antenna current that drives them. The signals from the detector(s) are mixed with reference signals from the rf generator to yield the in phase and quadrature (real and imaginary) components. From these the relative phase and amplitude of the density fluctuations are calculated.

3. RESULTS

Figure 2 shows a set of resonance curves calculated for the TCA parameters already mentioned for a deuterium plasma and an rf

frequency of 2.5 MHz. Waves with (n,m) = (2,1) and (2,-1) are directly excited by the usual (N,M) = (2,1) antenna phasing configuration, and the (n,m) = (2,0) and (2,2) waves are excited via toroidal coupling (APPERT et al., 1985). As the density increases, the radius at which the resonance condition (Eq. 1) is satisfied moves outwards. Figure 2 also shows the antenna loading and the rf wavefield component $\tilde{b}_\theta$ measured in the scrape-off layer. They exhibit a discrete spectrum in addition to the featureless continua defined by the resonance curves. The discrete peaks are due to the excitation of global modes just below the thresholds of continua with the same poloidal and toroidal mode numbers. At the bottom of the figure we show the amplitude and phase of the synchronous density fluctuations detected for a viewing chord at x/a = 0.4, during a discharge into which approximately 50 and 300 kW of rf power were delivered to the plasma at the (2,0) and (2,1) continua respectively. The signals are seen to peak at densities above those corresponding to the discrete loading peaks, signaling the passing of the resonance layers, which sweep outwards accross the viewing chord as the density rises. The decreasing phase indicates that at the high density side the wave is retarded with respect to its low density side. This observation was the first evidence confirming the predicted inward direction of propagation of the KAW.

Figure 3 summarises the results of an experiment in which the waves were excited with various combinations of antenna phasings. The detector viewed a chord at x/a = 0.33 and the spectrum was scanned by the increase of the density during the 60 ms rf pulse. Waves which do not correspond to a significant loading are found to have a low level of fluctuation. The importance of toroidal coupling, deduced from the

loading measurements by APPERT et al., (1985) is confirmed. An (N,M) antenna phasing structure also excites waves with m = M ± 1. The appearance and disappearance of the resonant surfaces for different excitation structures demonstrates that the toroidal mode purity seen in the discrete spectrum from the loading measurements by COLLINS et al., (1986) also holds in the continuum. The (n,m) = (4,-1) wave is of particular interest because, due to the sign of helicity, m/n < 0, no (4,-1) Discrete Alfvén Wave is observed, showing that these fluctuations appear independently of the discrete spectrum.

The localised radial wave structure and its inward direction of propagation are demonstrated in detail in Fig. 4 obtained from a series of 20 reproducible discharges in hydrogen, in which the detector position was scanned from shot to shot (antenna current 630 A peak, 100 kW coupled to the plasma, $\bar{n}_e = 3.5 \times 10^{19}$ m^{-3}). In the contour plot, Fig. 5, we see the detected amplitude as a function of the detector position and plasma density for the same discharges, shown together with the wavefronts (dashed, half-wavelength spacing). The amplitude is peaked near the estimated (2,0) and (2,-1) resonant layer positions (solid lines). The resonant positions were estimated using modelled profiles of the form $(1 - r^2/a^2)^K$, with K_n=0.7, K_j=2.4 and q(0)=0.95. Initial measurements of the (4,-1) continuum in a deuterium plasma show a similar evolution of the fluctuations as a function of density, Fig. 6. Unlike the case of the (2,0) continuum, the fluctuation level at this threshold is almost zero for the central chord. Moreover the waves oscillate in counterphase on either side of the magnetic axis, whereas for the (2,0) case they are mostly in phase. This is due to the difference in poloidal mode number parity.

In Fig. 6 we see that waves with (n,m)=(4,-2) and (4,-3) are excited in the edge region. Thus the waves associated with three different resonance layers can interfere, leading to the rather complicated wave pattern seen in the figure.

Sawtooth activity modulates the amplitude and the phase of the waves. The fine spikes affecting the curves on Fig. 3 are due to sawteeth. In the example of Fig. 7 the modulation of $\tilde{n}_e$ is compared with a centrally viewing soft x-ray signal. The plasma current and the density ($\bar{n}_e = 4.6 \cdot 10^{19} m^{-3}$) were constant for the first 20 ms of the rf pulse. A detailed investigation of the effect of sawtooth activity will require a multi-element detector array to probe the entire image field. This sensitivity to changes in the plasma profiles shows that the excitation and detection of the KAW can be exploited for diagnostics purposes, as originally proposed by ROSS et al. (1982).

A summary of the features of those KAW waves studied up to now under various conditions is given in Table 1. The radial wavelengths (Λ) are understood as the distance required to complete a full cycle (2π phase shift) and are evaluated in the vicinity of the maxima of amplitude. (For r < 5cm, the wavelengths are too long to be evaluated over a full cycle.) We notice that for a given mode, (2,0), the wavelength is shorter for a hydrogen plasma than for a deuterium plasma as expected from the smaller ion Larmor radius. We also see that waves associated with resonance layers closer to the edge ($r/a \approx 0.75$) have a shorter wavelength than those observed close to the centre. This can be understood from Eq. (2) with the lower temperatures and steeper gradients near the edge. Figure 8 shows the range of wavelengths observed as a function of the position of the viewing chord and an

estimate of Λ by Eq. (2) using modelled density and temperature profiles. We see that the predicted wavelengths are in reasonable agreement with the experimental observations.

These results are in qualitative agreement with the simulations of ROSS et al., (1982) and DONNELLY et al., (1986b), for comparable plasma conditions. A comparison between our experimental results and predictions by a cylindrical kinetic code will be the subject of a later publication.

4. CONCLUSION

Using a novel laser diagnostic specifically built for this purpose, we have revealed the presence, at the Shear Alfvén resonance layers, of driven density fluctuations that have the features of the Kinetic Alfvén Wave. They propagate inwards and their wavelengths are reasonably well predicted by the WKB approximation. We have confirmed the selective excitation of the different resonance layers using the TCA modular antenna structure.

ACKNOWLEDGEMENTS

We gratefully acknowledge the support of our colleagues of the TCA Team, as well as stimulating discussions with Dr. K. Appert and Prof. F. Troyon. This work was partially supported by the Fonds National Suisse de la Recherche Scientifique.

REFERENCES

APPERT K., COLLINS G.A., HOFMANN F., KELLER R., LIETTI A., LISTER J.B., POCHELON A., VILLARD L. (1985) Phys. Rev. Lett. 54, 1671.

APPERT K., COLLINS G.A., HELLSTEN T., VACLAVIK J.,VILLARD L. (1986) Plasma Phys. and Contr. Fusion 28, 133.

COLLINS G.A., HOFMANN F., JOYE B., KELLER R., LIETTI A., LISTER J.B., POCHELON A. (1986) Physics Fluids, in press.

DONNELLY I.J., CLANCY B.E., BRENNAN M.H. (14-18 April 1986a) 13th European Conference on Controlled Fusion and Plasma Heating, Schliersee.

DONNELLY I.J., CLANCY B.E., CRAMER N.F. (1986b) J. Plasma Phys., 35, 75.

JOYE B., LIETTI A., LISTER J.B., MORET J.-M, SIMM W.C. (1986), PHYS. REV. LETT. 56, 2481

HASEGAWA A., CHEN L. (1975) Phys. Rev. Lett. 35, 370.

HASEGAWA A., CHEN L. (1976) Physics Fluids 19, 1924.

ROSS D.W., CHEN G.L., MAHAJAN S.M. (1982) Physics Fluids 25, 652.

WEISEN H. (1985) Infrared Physics 25, 543.

WEISEN H. (10-12 Sept. 1985) Proc. 2nd Int. Symposium on Laser-Aided Plasma Diagnostics, Culham.

WEISEN H. (1986) Plasma Phys. and Contr. Fusion, in press.

FIGURE CAPTIONS

FIG. 1—Schematic of the optical system showing the refractive perturbation due to the KAW and the resulting intensity variations in the image plane.

FIG. 2—The Alfvén wave spectrum excited in TCA under typical conditions.

FIG. 3—The driven density fluctuations observed with various combinations of antenna phasings.

FIG. 4—Fluctuation profile in the (n,m)=(2,0) continuum a) amplitude, b) phase.

FIG. 5—Evolution of the radial structure of the driven density oscillations as the density increases (contours of equal amplitude). Wavefronts spaced by π in phase are shown as dashed lines. The thick lines show the expected resonant positions for modelled profiles. (N,M) = (2,1), hydrogen.

FIG. 6—As Fig. 5, but (N,M) = (4,1), deuterium.

FIG. 7—Modulation of the density fluctuations by sawtooth activity. (P_{rf}=16kW, x/a=0.42)

FIG. 8—Range of radial wavelengths observed as a function of radial position.

TABLE 1—Summary of features of the KAW's investigated.

TABLE 1

(n,m)	fill	range of x [cm]	range of Λ [cm]	FWHM [cm]	$\bar{n}_e$ [10^{19} m^{-3}]
(2,0)	H	5 - 11	3.5 - 4.5	~ 3.5	3.3 - 3.9
(2,0)	D	7 - 12	4 - 5.5	~ 5	2.2 - 2.6
(4,-1)	D	5 - 9	4 - 6		5 - 6
(2,1)	D	5 - 9	4 - 6		~ 4.5
(2,-1)	H	10 - 14	2.7 - 3.2	~ 3.5	2.2 - 2.7
(4,-3) (4,-2)	D	12.5 - 14	2.5 - 3.5		3.8 - 6

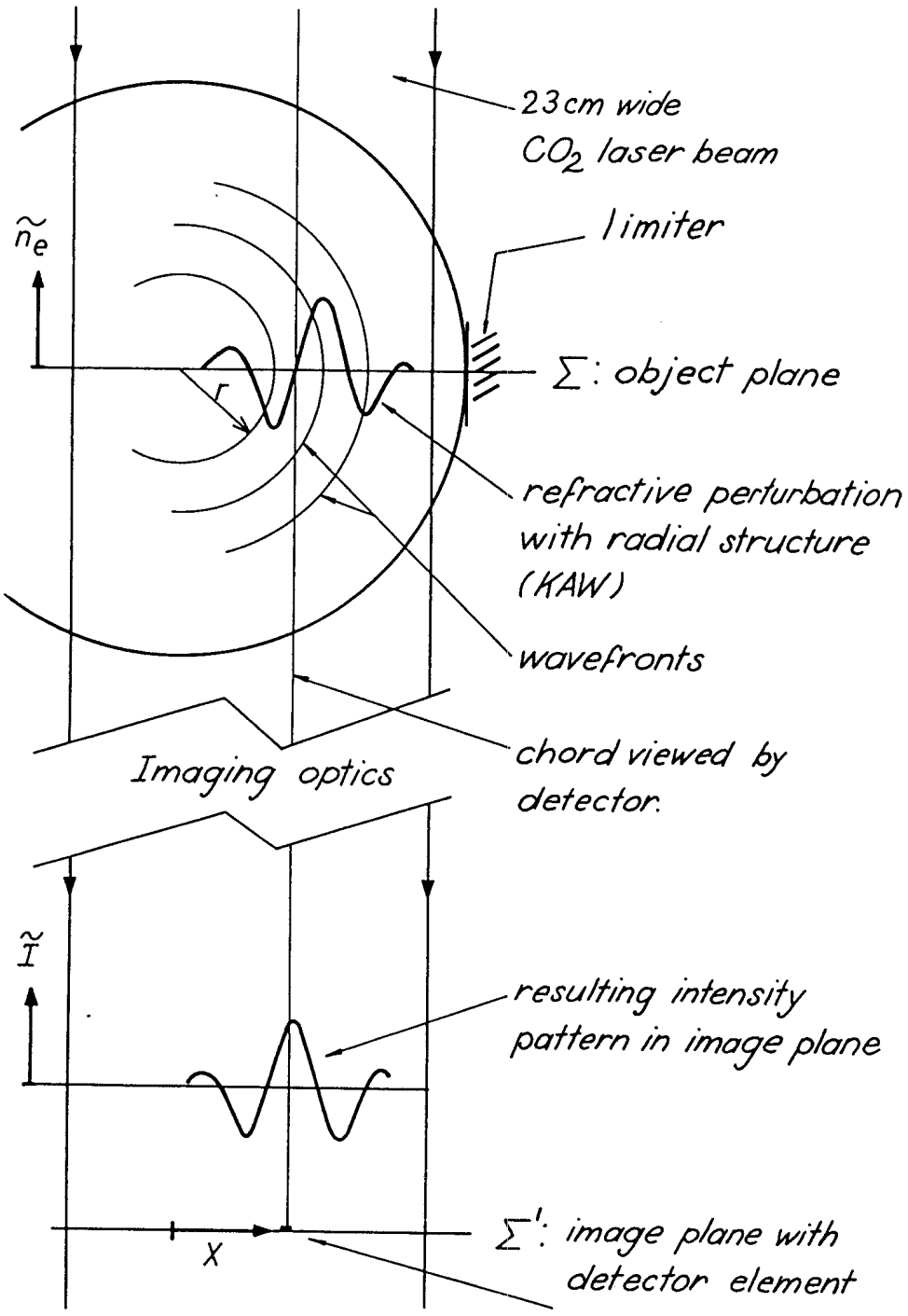
23cm wide
CO_2 laser beam
limiter
$\tilde{n}_e$
Σ: object plane
r
refractive perturbation
with radial structure
(KAW)
wavefronts
chord viewed by
detector
Imaging optics
$\tilde{I}$
resulting intensity
pattern in image plane
Σ': image plane with
detector element
X

FIG. 1

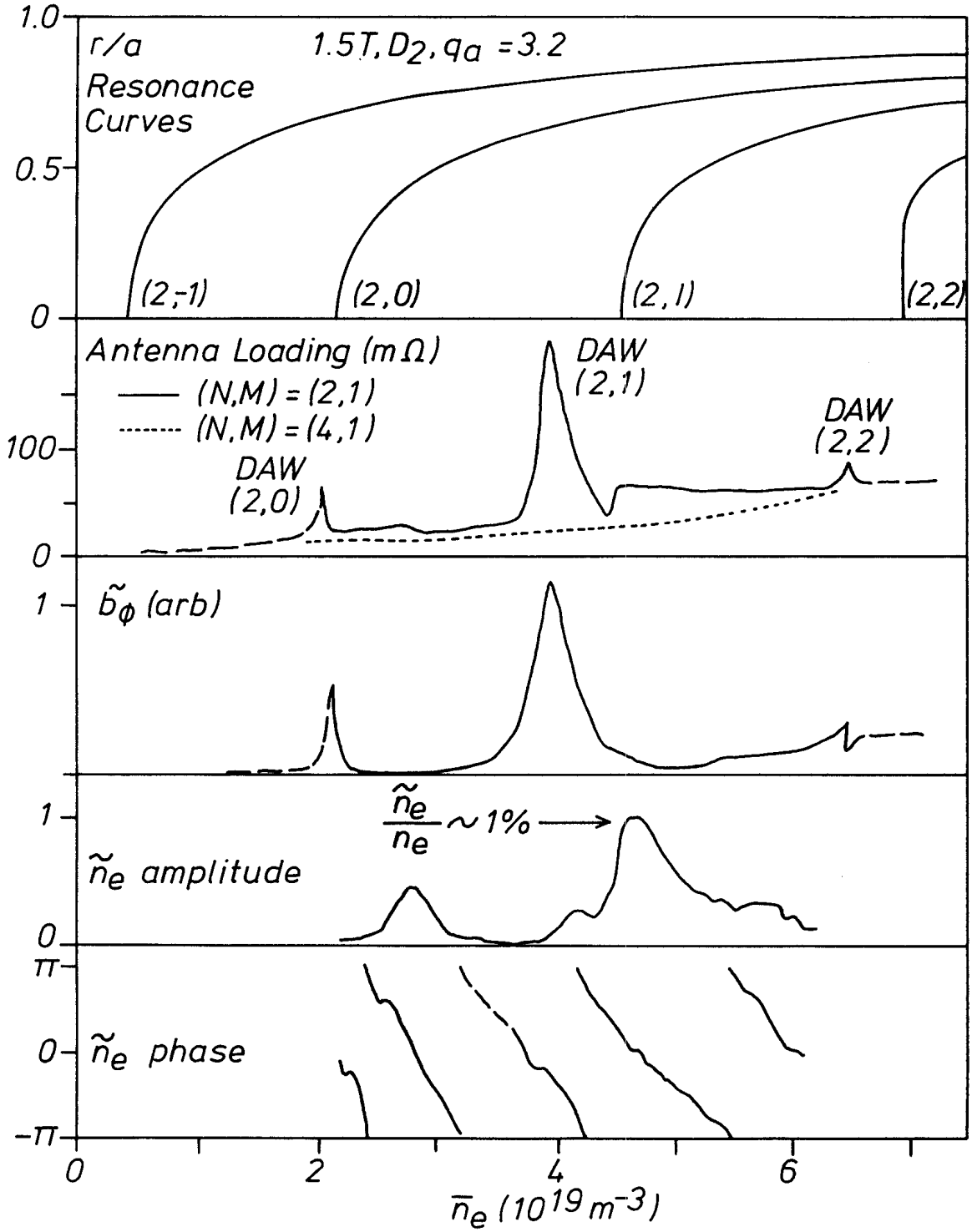
1.0
r/a
1.5T, D_2, q_a = 3.2
Resonance
Curves
0.5
0
(2,-1)
(2,0)
(2,1)
(2,2)
Antenna Loading (mΩ)
(N,M) = (2,1)
(N,M) = (4,1)
DAW
(2,1)
DAW
(2,2)
DAW
(2,0)
100
0
1
$\tilde{b}_\phi$ (arb)
1
$\frac{\tilde{n}_e}{n_e} \sim 1\%$
$\tilde{n}_e$ amplitude
0
π
0
$\tilde{n}_e$ phase
-π
0
2
4
6
$\bar{n}_e$ (10^{19} m^{-3})

FIG. 2

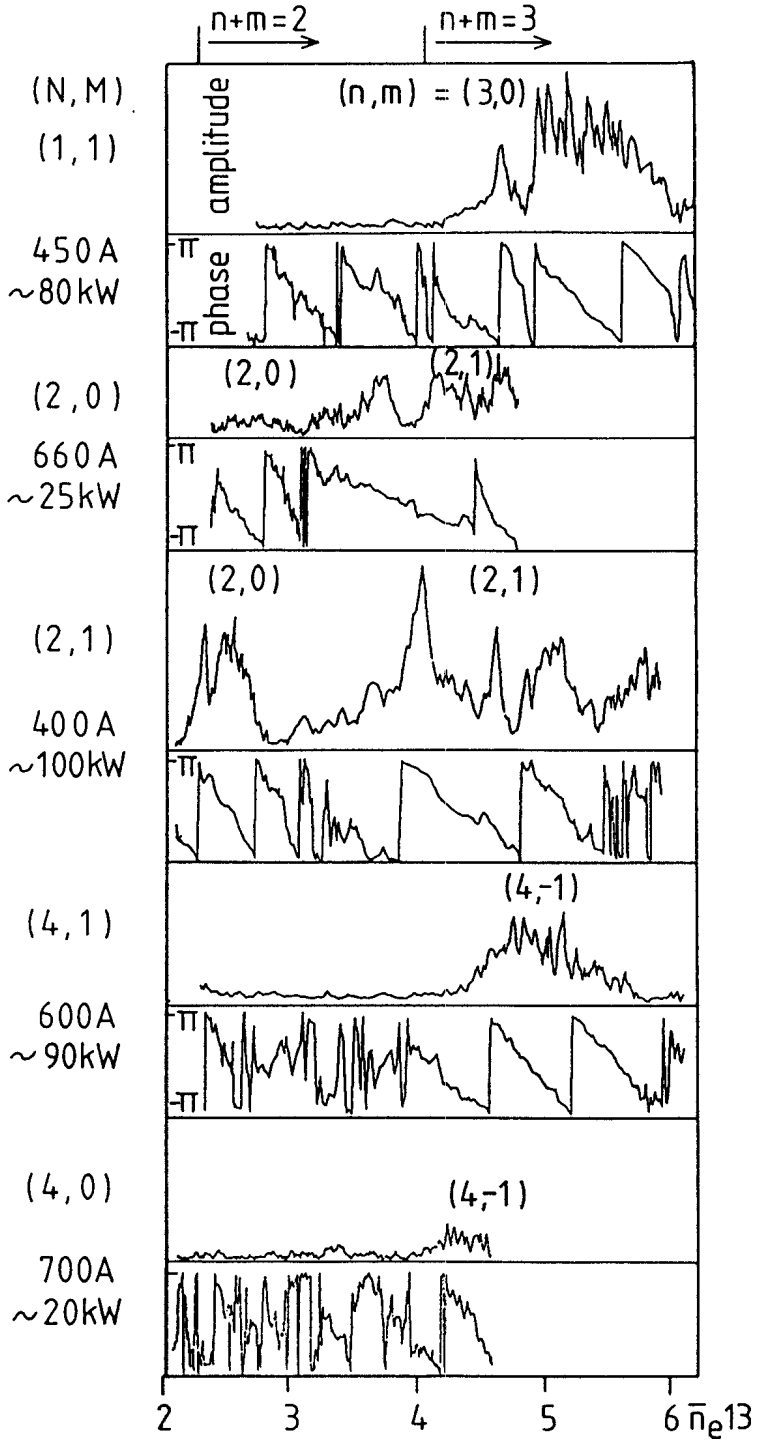
n+m=2
n+m=3
(N, M)
(1, 1)
amplitude
(n,m) = (3,0)
450 A
~80kW
phase
(2,0)
(2,1)
(2, 0)
660 A
~25kW
(2,0)
(2,1)
(2, 1)
400 A
~100kW
(4,-1)
(4, 1)
600A
~90kW
(4, 0)
(4,-1)
700A
~20kW
2
3
4
5
6 $\bar{n}_e 13$

FIG. 3

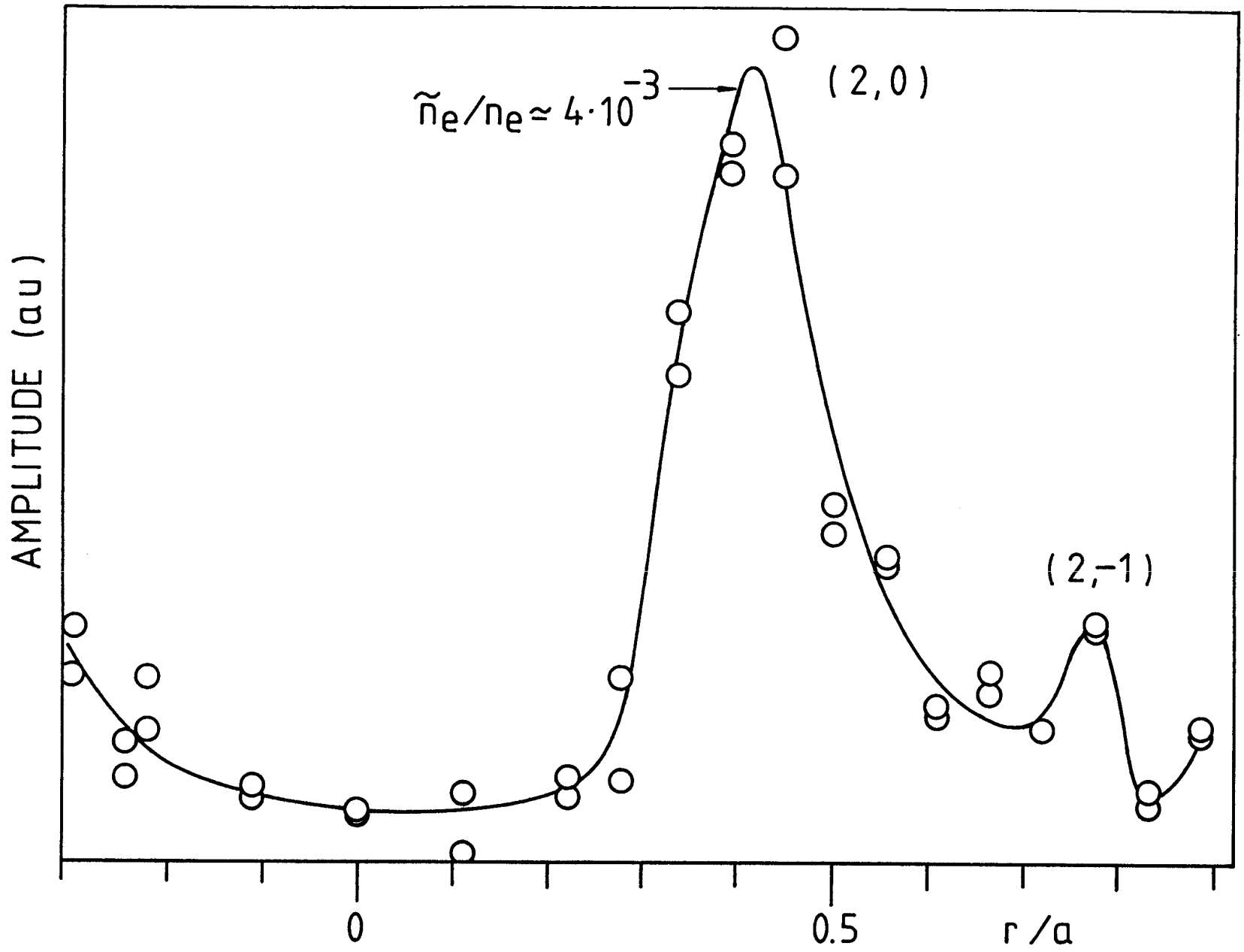

FIG. 4a

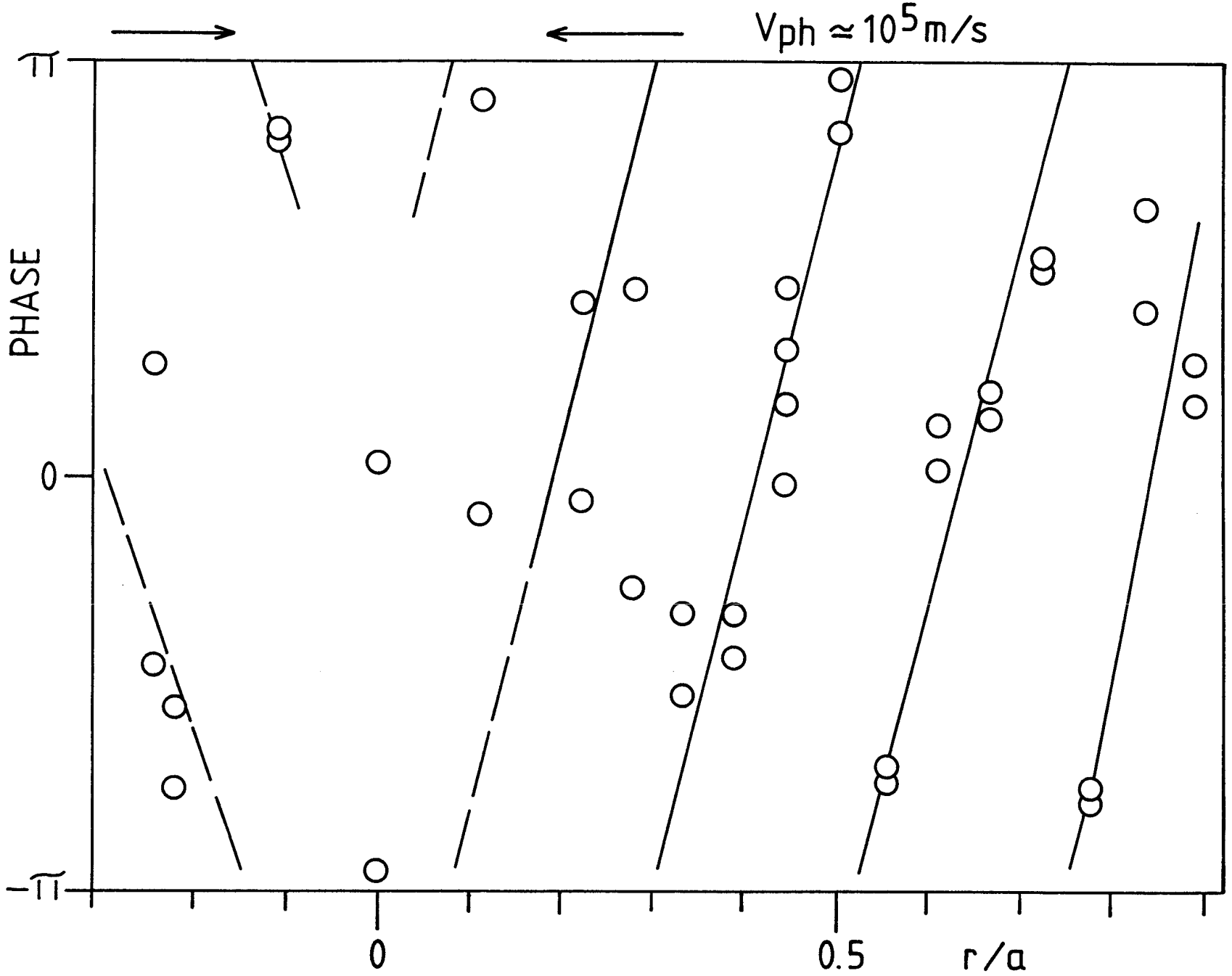

FIG. 4b

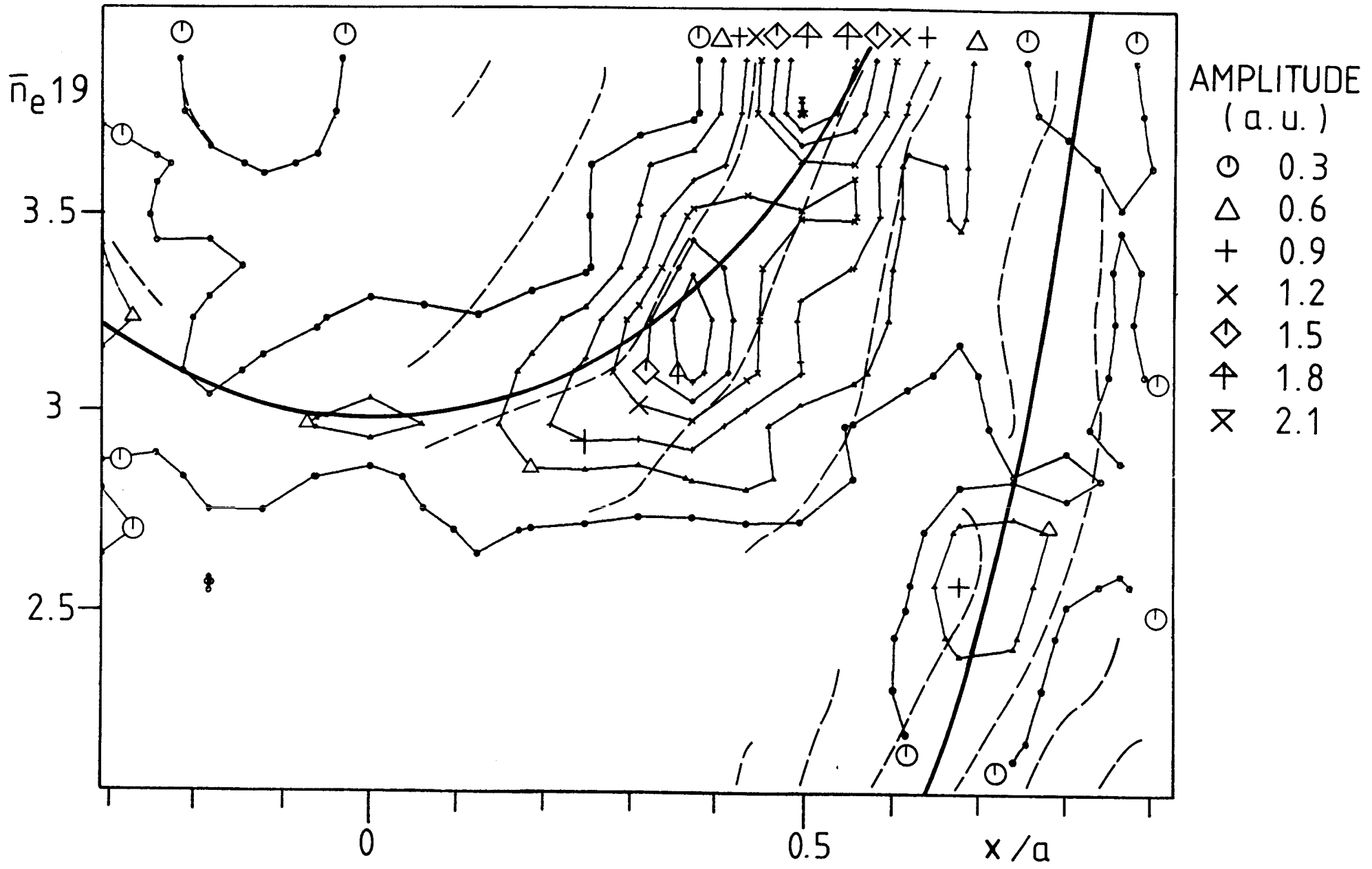

FIG. 5

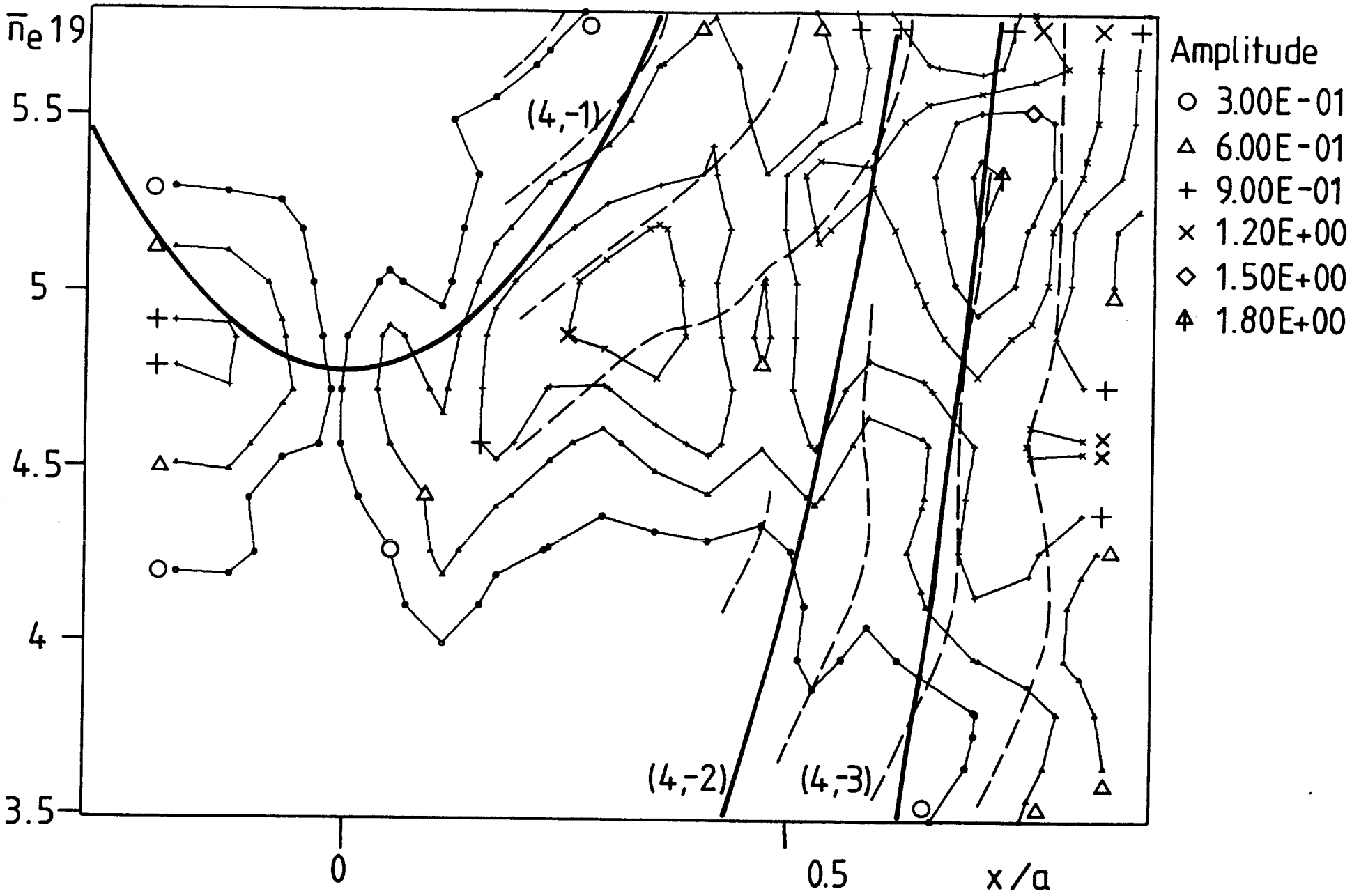
$\bar{n}_e$ 19
5.5
5
4.5
4
3.5
0
0.5
x/a
(4,-1)
(4,-2)
(4,-3)
Amplitude
3.00E-01
6.00E-01
9.00E-01
1.20E+00
1.50E+00
1.80E+00

FIG. 6

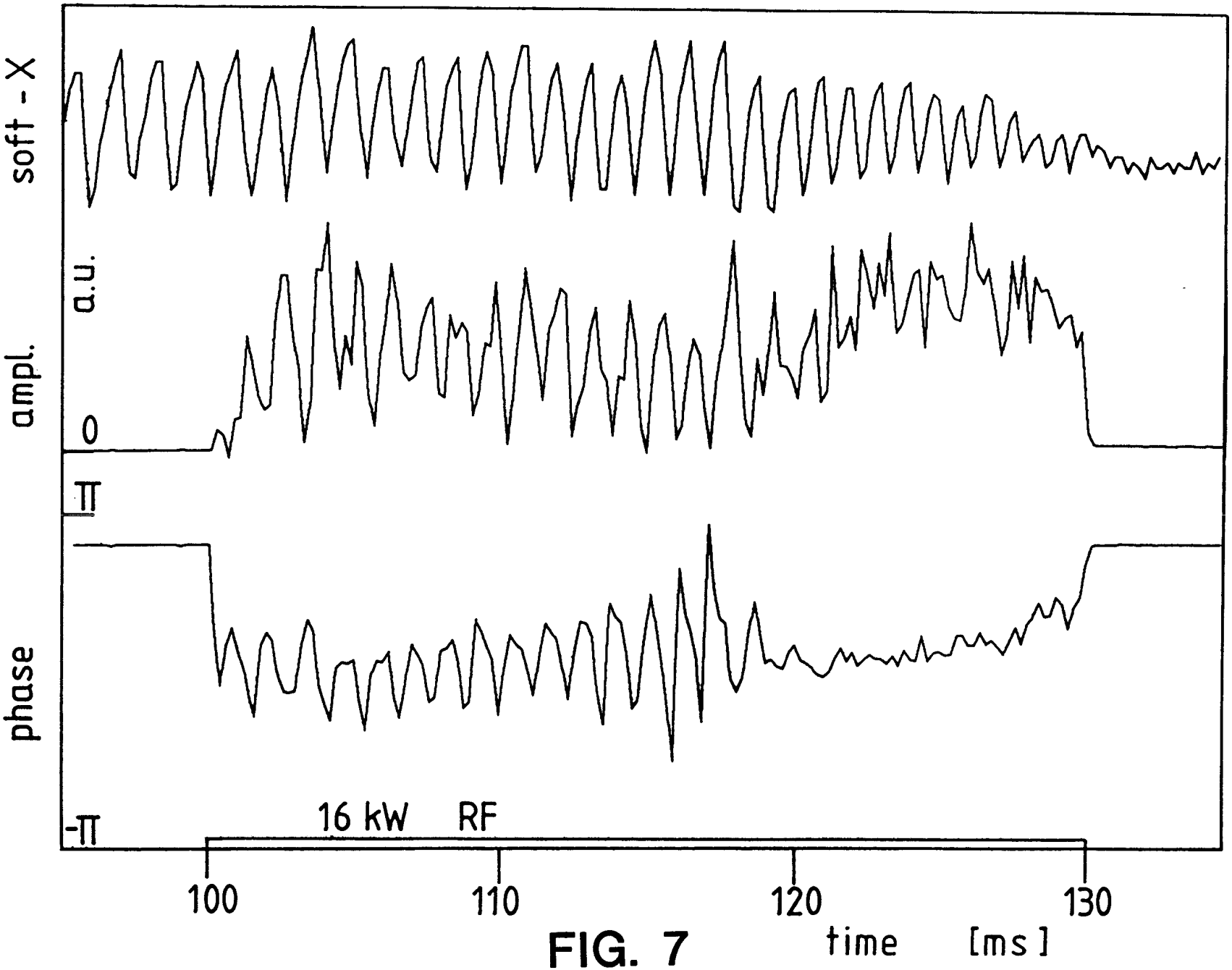

FIG. 7

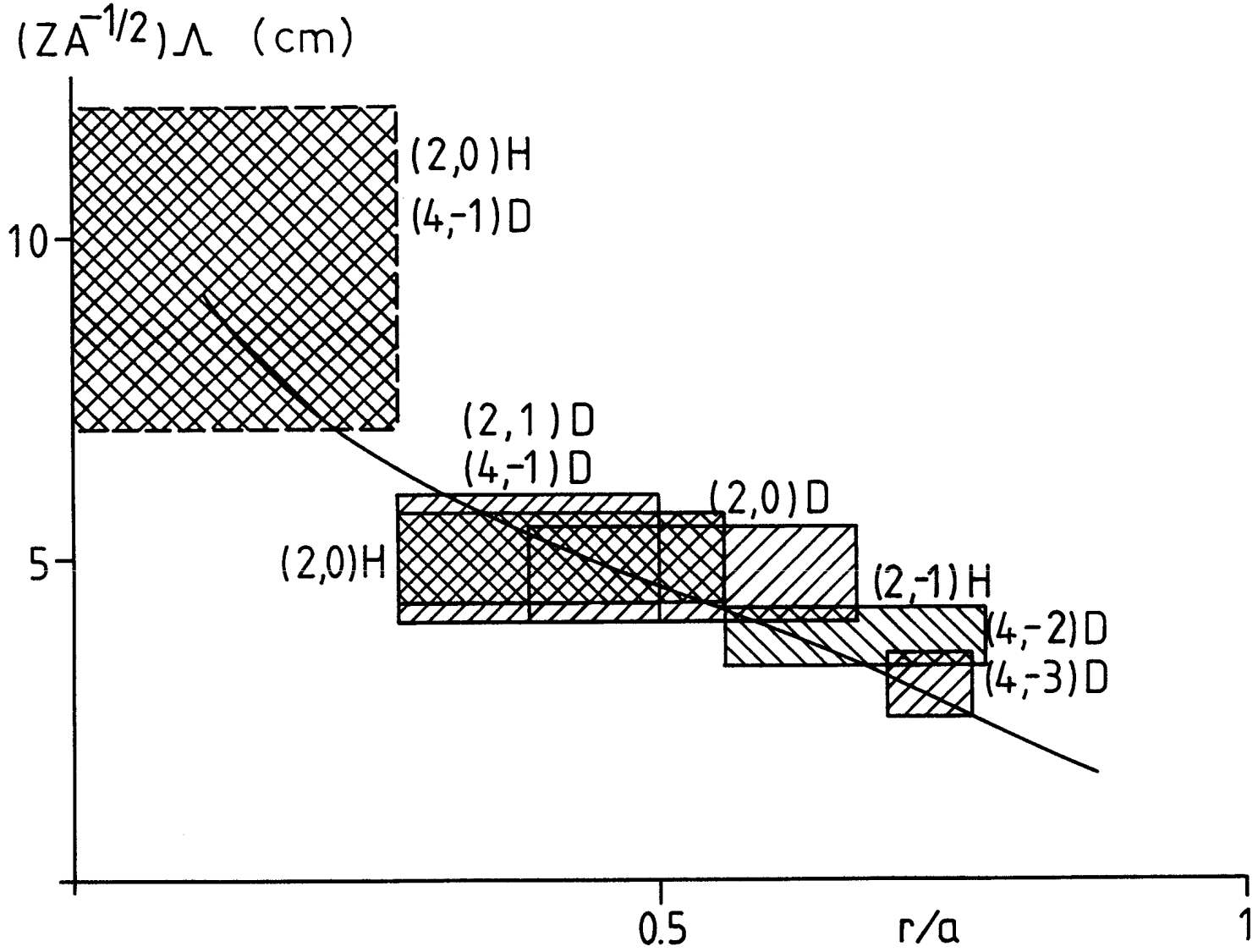

FIG. 8